



Design and evaluation of an anthropomorphic neck phantom for improved ultrasound diagnostics of thyroid gland tumors

Denis Leonov^{1,2} · Anastasia Nasibullina¹ · Veronika Grebennikova^{1,2} · Olga Vlasova¹ · Yulia Bulgakova^{1,2} · Ekaterina Belyakova^{1,3} · Darya Shestakova⁴ · José Francisco Silva Costa-Júnior⁵ · Olga Omelianskaya¹ · Yuriy Vasilev¹

Received: 9 January 2024 / Accepted: 27 March 2024
© CARS 2024

Abstract

Purpose Thyroid cancer is one of the most common cancers worldwide, with ultrasound-guided biopsy being the method of choice for its early detection. The accuracy of diagnostics directly depends on the qualifications of the ultrasonographers, whose performance can be enhanced through training with phantoms. The aim of this study is to propose a reproducible methodology for designing a neck phantom for ultrasound training and research from widely available materials and to validate its applicability.

Methods The phantom was made using polyvinyl chloride mixed with additives to reproduce different levels of brightness on ultrasound screens. 3D printing and casting were used to create the neck model and various structures of the neck, including bones, cartilage, arteries, veins, lymph nodes, thyroid gland, and soft tissues. The small objects, such as tumor and lymph node models, were shaped manually. All the phantom's materials were carefully selected to match the ultrasonic speed and attenuation values of real soft tissues and bones.

Results The thyroid gland contains models of a cancerous and cystic nodule. In the neck, there are models of carotid arteries and jugular veins filled with ultrasound-transparent gel. Additionally, there are replicas of lymph nodes and bone structures such as hyoid bone, thyroid cartilage, trachea, and vertebrae. The resulting phantom covers the entire neck area and has been positively received by practicing ultrasound specialists.

Conclusions The proposed manufacturing technology offers a reliable and cost-effective approach to produce an anthropomorphic neck phantom for ultrasound diagnosis of the thyroid gland. The realistic simulation provided by the phantom enhances the quality and accuracy of ultrasound examinations, contributing to better training for medical professionals and improved patient care. Subsequent research efforts can concentrate on refining the fabrication process and exploring additional features to enhance the phantom's capabilities.

Keywords Training phantom · Anthropomorphic neck phantom · Ultrasound diagnosis · Thyroid gland · Tissue-imitating materials · PVC plastisol · 3D modeling · Fabrication technology

Introduction

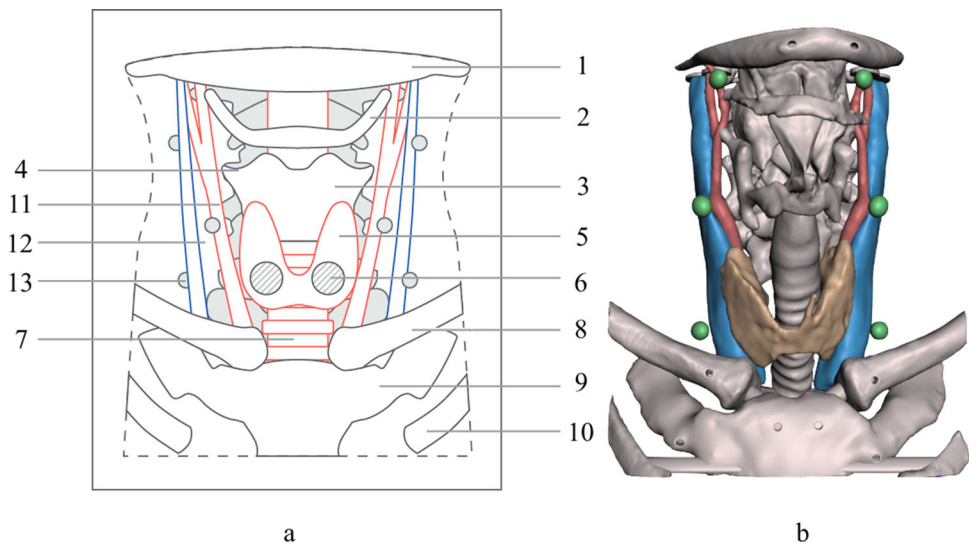
Over the past 25 years, the incidence of thyroid cancer has increased more than threefold, solidifying its status as one of the most prevalent diseases globally [1]. Ultrasound diagnostics emerges as the most effective, non-invasive, and accessible method for early detection of tumor formations in the thyroid gland, providing precise guidance for fine-needle biopsies. However, the accuracy of ultrasound procedures directly depends on the qualifications of the performing

physicians. Therefore, there is a critical need to prioritize the training of highly skilled specialists, who can adeptly apply theoretical knowledge in practice. This objective can be achieved through the widespread implementation of training phantoms [2].

Commercially available phantoms produced by CIRS and Blue Phantom are expensive and therefore inaccessible for many students and training centers. Promising designs of ultrasonic thyroid phantoms have been presented in recent studies [3–8]. Some researchers create low-cost phantoms using perishable materials such as ballistic gel, chicken

Extended author information available on the last page of the article

Fig. 1 Scheme (a) and segmented parts (b) of the neck phantom: 1—mandible; 2—hyoid bone; 3—thyroid cartilage; 4—cervical spine; 5—thyroid gland; 6—thyroid nodules; 7—trachea; 8—clavicle; 9—sternum; 10—ribs; 11—arteries; 12—veins; 13—lymph nodes



breast, fruits, and olives [4–7]. Others implement 3D printing technology achieving a sufficient level of accuracy for the model [8]. However, the low-cost phantoms have short durability, do not realistically mimic thyroid anatomy, lack reproducibility, and the 3D-printed design requires expensive Stratasys machines.

The aim of this study is to propose and validate a reproducible methodology for designing a neck phantom for ultrasound training and research using widely available materials and equipment. The proposed design utilizes polyvinyl chloride (PVC) as a base material due to its longevity and acoustic properties being close to human tissues [9]. The phantom accurately reproduces ultrasound anatomy of the human neck and is suitable for ultrasound diagnostics and elastography training, as well as practicing fine-needle aspiration techniques.

Materials and methods

By introducing various additives to the PVC (graphite powder, metallic glitter), we were able to reproduce different levels of brightness on the screen of ultrasound scanners [9]. This approach combined with 3D printing, allowed for the reconstruction of various structures in the neck, including bones, cartilage, arteries, veins, lymph nodes, thyroid gland, anomalous thyroid objects, as well as soft tissues with skin.

As a preliminary step, we meticulously studied the neck anatomy, creating schematic representation of the anatomical landmarks of the neck phantom, as depicted in Fig. 1a. Subsequently, angiographic computed tomography data from neck examinations were imported into 3D Slicer software, and all the neck organs were segmented. The results of this segmentation are presented in Figs. 1b and 2a–d. In detail, the manufacturing process was the following. The neck shape

was segmented from computed tomography and 3D printed with an Anycubic Photon M3 Max (China) using LCD (liquid crystal display) technology and Industrial Blend resin (Fun-to-do, the Netherlands). The 3D-printed neck model was used to create the casting mold from tin-based liquid silicone (KREMEN MOLD 10, Russia). The printed neck model was placed in the silicone, and the silicone solidified, resulting in a reusable, heat-resistant casting mold. The creation of the phantom itself went through several stages: the production of composite parts, including bones, thyroid gland with lesions, blood vessels, lymph nodes, and the casting of soft tissue models with the inserted composite parts. Tumor and lymph nodes were made of pure PVC without any additives and with the addition of 100 μm large particles of metallic glitter in a small concentration, respectively. They were then manually processed to give them a specific size and shape. Virtual models of the molds for casting vessels and the thyroid gland were made using Meshmixer, a manual 3D modeling software, and then 3D printed, as shown in Fig. 2e–g. Bone and cartilage models were segmented from CT scans of patients and also 3D-printed, as seen in Fig. 2a and h. Vessels were filled with pure PVC, and the thyroid gland was filled with PVC with admixtures of 0.5% metallic glitter and 1% graphite powder (Fig. 2i–k). To cast the phantom, an admixture was added to the material in advance, and it was degassed to prevent air accumulation.

Table 1 describes the required consumables to create a single thyroid phantom. In order to create a single phantom, one must purchase materials costing a total of \$137.84. However, as the most costly components are only utilized for making molds, the overall direct manufacturing cost decreases to \$32.72 per unit when producing 100 copies. The production of a single thyroid phantom, excluding mold manufacturing, required a total of 55 h. This includes 9 h dedicated to the 3D printing of bone models, 8 h for the creation of vessels,

Fig. 2 Illustrations of the manufacturing of the neck phantom: segmented from angiographic computed tomography data virtual models of bone structures (a), carotid arteries (b), veins (c), thyroid gland (d); casting molds for arteries (e), veins (f), and thyroid gland (g); 3D printed bone structures (h); carotid artery (i), vein (j), and thyroid gland (k) after extraction from the molds

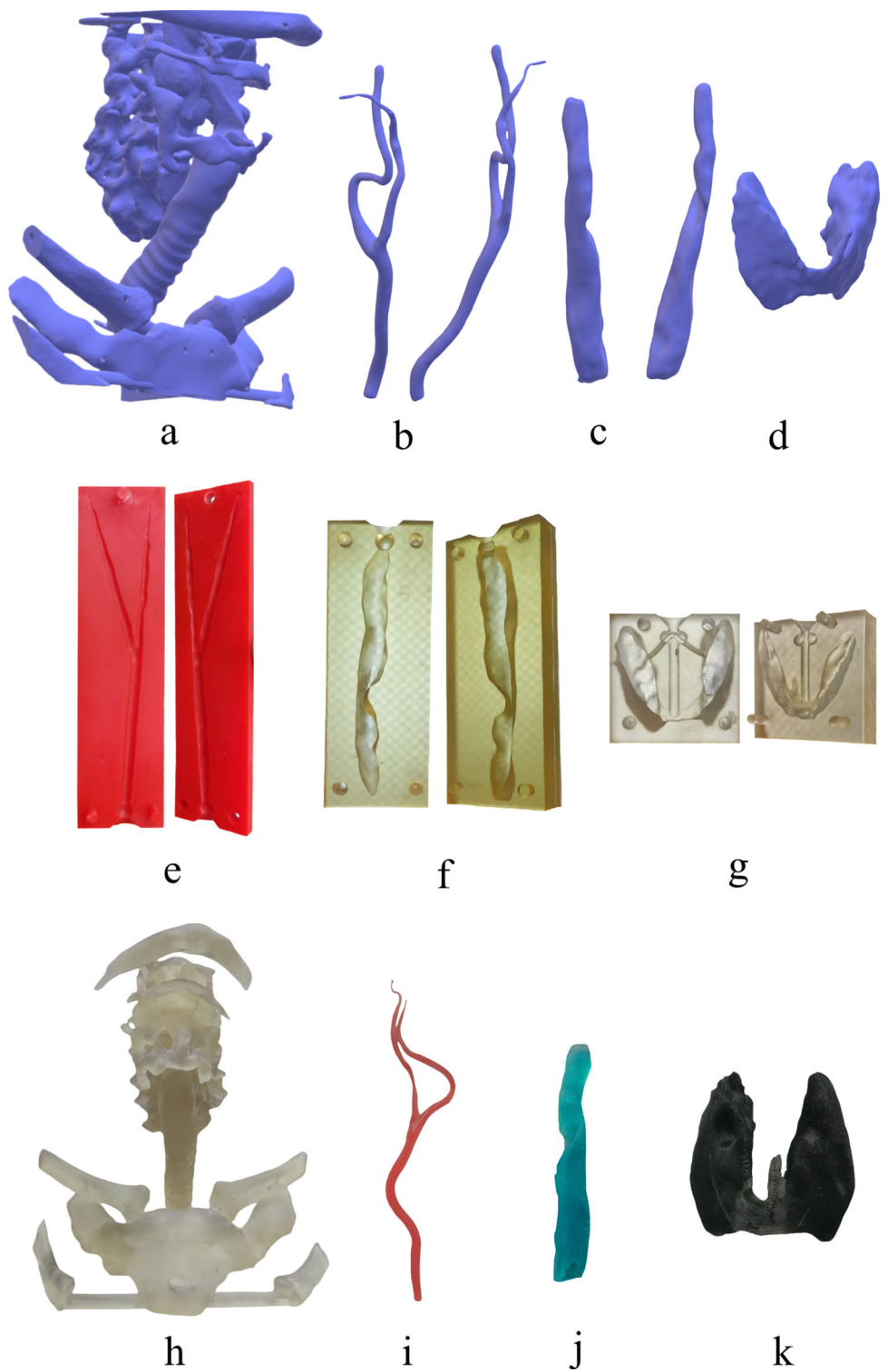


Table 1 Materials for making a thyroid phantom

Material	Price	Actual consumption
To make the phantom itself		
1. PVC	\$6.94 / 1000 ml	2950 ml
2. Glitter	\$1.32 / 20 g	19 g
3. Dye	\$1.6 / 50 ml	7 ml
4. Flavoring	\$2.53 / 50 ml	11 ml
5. Photopolymer resin	\$23.72 / 1000 g	400 g
To make a mold for filling (done once every 100 copies)		
1. Photopolymer resin	\$23.72 / 1000 g	1150 g
2. Silicone	\$13.47 / 1000 g	2500 g

lymph nodes, tumors, and a thyroid gland, and 10 h for the assembly of all individual models within the phantom. The remaining time was needed for the cooling of the final product. The manufacturing of molds, including 3D printing and silicone casting, takes at least another 55 h.

In order to select materials and admixtures, an experiment was conducted to measure the speed and attenuation coefficient of ultrasonic waves. The experiment used a method outlined in [9] to study the transmission of waves through solid media. The setup included an ultrasound source and a hydrophone attached to a sample of PVC plastisol. Ultrasonic signals were generated and collected by an IntroVisor ultrasonic flaw detector (ACS Group, Saarbrücken, Germany) with sensors emitting bursts at carrier frequencies between 1 and 10 MHz with 25 V and a pulse repetition frequency of 10 Hz. Measurements were taken with sensors placed coaxially at different distances between them to determine ultrasonic speed and attenuation. The parameters were measured in samples of pure PVC plastisol as well as with the admixtures of 0.5% metallic glitter and 1% graphite powder. The resulting values for each material were determined by averaging five measurements.

The phantom underwent examination with linear probes on the various ultrasound scanners: Medison Sonoace 8000 EX Prime (Medison Co., Seoul, South Korea) operating in B-mode; Ruscan 65 M (RPA “Scanner,” Moscow, Russia) with LA3-14AD linear probe operating at central frequency of 9.4 MHz (B-mode); Sonomed-500 (Spectromed, Moscow, Russia) using 7.5L38 probe; Angiodin Sono/P-Ultra (BIOS, Moscow, Russia) with L5-12/40 linear probe operating at central frequency of 7.5 MHz (sonoelastography mode); and BK Specto Ultrasound (BK medical, Herlev, Denmark) with 14L3e linear probe operating at central frequency of 9 MHz (B-Mode); Mindray M9T (Mindray, Shenzhen, PRC) with L14-6Ns probe. All images were analyzed at depths ranging from 30 to 70 mm. Using each of the scanners, an ultrasonographer with 7 years’ of experience captured and stored

three images for each model inside the phantom in a manner ensuring the visibility of their borders. The echogenicity and clarity of the borders for each part of the phantom were visually assessed by the ultrasonographer. In order to provide quantitative comparisons, the dimensions of structures within the phantom were measured at different stages. Initially, measurements were taken during the virtual modeling stage just after segmentation of the patient’s computed tomography images. Following this, a micrometer was employed to assess the dimensions of PVC plastisol models prior to their incorporation into the phantom. Ultimately, the dimensions of the models in sonograms were measured using the built-in measuring device of ultrasound system. These results were then compared to data found in the literature.

To assess the impact of a fine-needle puncture, an experiment was conducted in which a G21 needle was inserted into phantom tissue samples 100 times. Ultrasound images were captured both before and immediately after the needle insertion, as well as 15 min later.

Results

The model was produced that covers the entire neck area, from the clavicles to the chin-neck junction, facilitating a comprehensive examination and study. A picture of the phantom taken with a Nikon D780 camera as well as its ultrasound images are presented in Fig. 3. In the presented images, one can observe a hyoid bone (2), thyroid cartilage (3), thyroid isthmus (5), nodule (6), trachea (7), artery (11), vein (12), and a lymph node (13). The phantom was evaluated and positively received by a practicing thyroid ultrasound specialist, highlighting the effectiveness of the PVC-based modeling approach. Figure 4 demonstrates several types of nodules that can be reproduced in the thyroid gland phantom using the proposed technology. Table 2 presents the measurements of the thickness of the structures modeled at various stages of production, obtained through the segmentation of computed tomography images, micrometer readings, and ultrasound images. Additionally, literature data are included for quantitative comparison.

Figure 5 illustrates the relationship between ultrasound speed and frequency for PVC plastisol samples containing various admixtures. The minimum and maximum levels of ultrasound speed in the human neck tissues were sourced from the literature. The data presented in Fig. 5 depict the spectrum of ultrasound speed values observed in both fatty and glandular tissues. Furthermore, an evaluation of attenuation at 1 MHz frequency was performed. In plastisol with a Shore stiffness of 3 units and no admixtures, the attenuation was measured at 0.32 dB/cm/MHz. This value increased to 0.58 dB/cm/MHz with the addition of 0.5% metallic glitter

Fig. 3 Photo (a) and sonograms (b–f) of the phantom simulating ultrasound anatomy of the human neck. Ultrasound images (b–f) were captured using Medison Sonoace 8000 EX Prime with the L5-9EC probe operating at the center frequency of 7.5 MHz. Image (g) was obtained with Sonomed-500 ultrasound scanner using the 7.5L38 probe. Images (h and i) were acquired with Midray M9T and the L14-6Ns probe. Numbers in images correspond to the scheme in Fig. 1

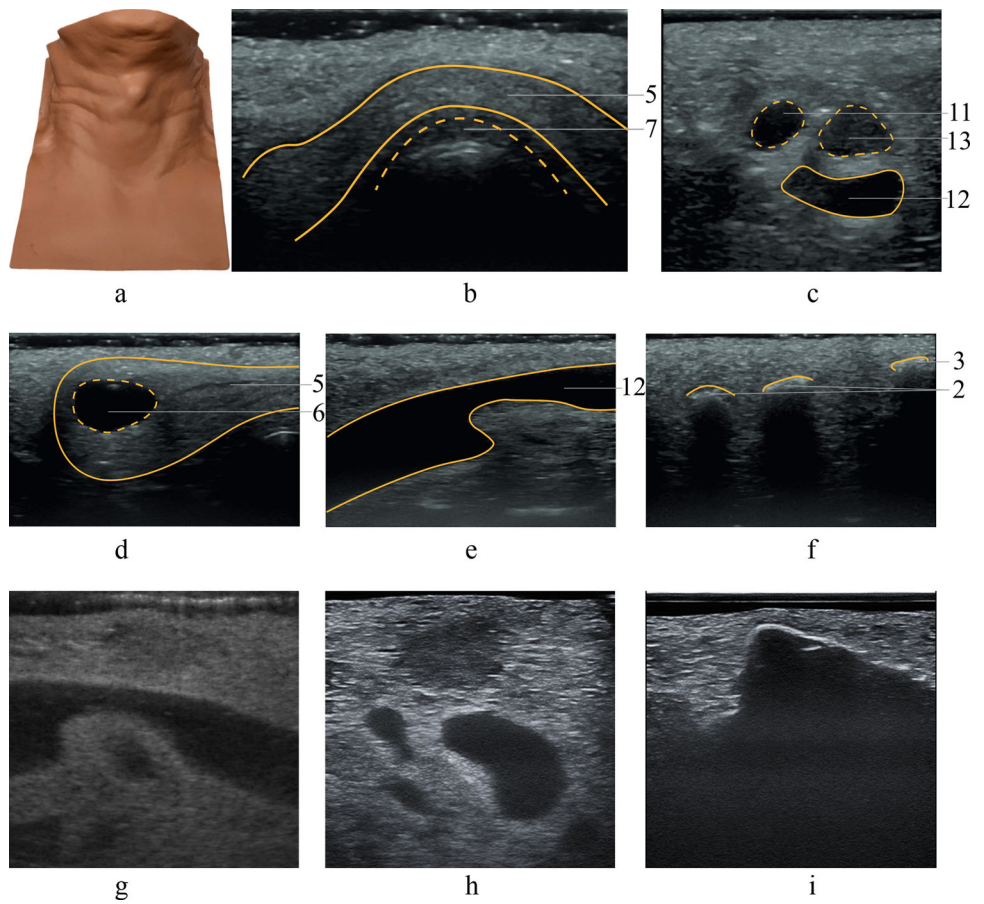
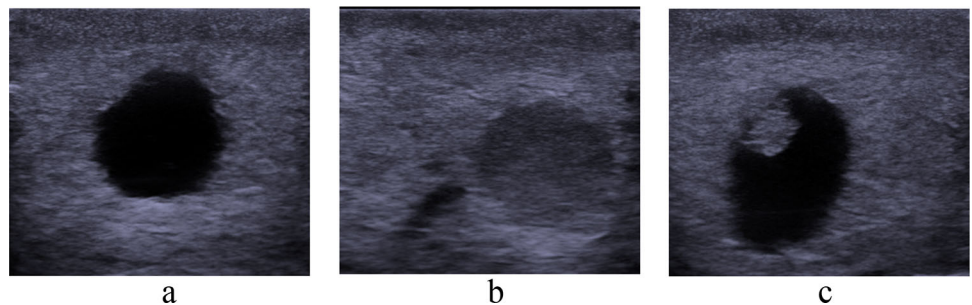


Fig. 4 Ultrasound images of cystic (a), solid (b), and cystic-solid (c) models of a thyroid gland nodule were captured with the BK Spectro Ultrasound machine (BK medical, Herlev, Denmark) using 14L3e linear probe operating at central frequency of 9 MHz



and 0.95 dB/cm/MHz with the combination of 1% graphite powder and 0.5% metallic glitter.

The results of the experiment, detailing the effects of needle puncture, are depicted in Fig. 6. The image (b) clearly shows the appearance of marks following the needle insertions, which in 15 min become significantly less prominent, thus demonstrating the self-healing capability of the tissue model.

Discussion

The necessity for physicians to have confidence in their thyroid ultrasound and fine-needle biopsy skills is essential

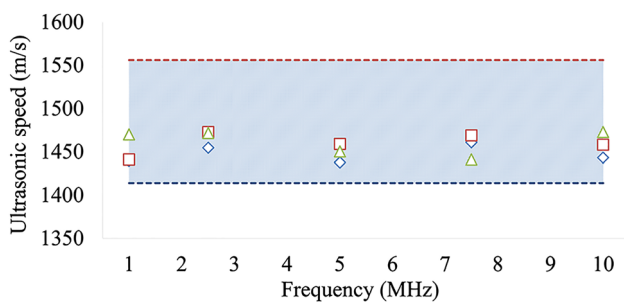
as the field progresses. It is both unethical and unsafe for trainees to perform invasive procedures on patients without adequate practice. To address this, simulation-based education has been proven effective in enabling trainees to acquire technical skills in a safe and controlled environment until they become proficient [2]. In this study, a thyroid phantom for ultrasound training has been developed.

The design is grounded in our prior research on phantom development using PVC [9, 13, 14]. Like the phantoms described earlier, our thyroid model is made using easily accessible materials and equipment, is inexpensive to produce, mimics the desired ultrasound anatomic features, and can be easily reproduced. However, what distinguishes this

Table 2 Quantitative comparison of the dimensions of modeled organs at the stages of: i) segmentation of computed tomography data; ii) PVC models casting; iii) ultrasound measurements of the phantom.

Modeled organ and its parameter	Dimensions at different stages, mm			
	i	ii	iii	Reference
Thyroid gland				
Isthmus	3.39	2.79	3.41	2–4
Left lobe				
Length	51.39	49.02	49.80	40–60
Width	15.42	15.50	16.90	12–18
Height	17.97	16.64	15.73	13–18
Volume*	6.82	6.06	6.34	6–9
Right lobe				
Length	50.05	47.16	51.34	40–60
Width	17.39	17.58	17.01	12–18
Height	17.21	15.18	14.67	13–18
Volume*	7.17	6.03	6.14	6–9
Carotid artery	6.94	7.74	5.80	4.2–6.0
Lymph node				
Normal	–	8.66	8.38	< 12
Swollen	–	14.07	13.74	12–25

Reference column contains literature data [10, 11]. Asterisks indicate that the volume is measured in cm³

**Fig. 5** Frequency dependence of ultrasound speed in the neck area (values obtained from [12]): (–) min, (–) max; (◇) pure plastisol from our experiments, (□) a mixture of plastisol and 0.5% metallic glitter, (△) a mixture of plastisol, 0.5% metallic glitter and 1% graphite powder

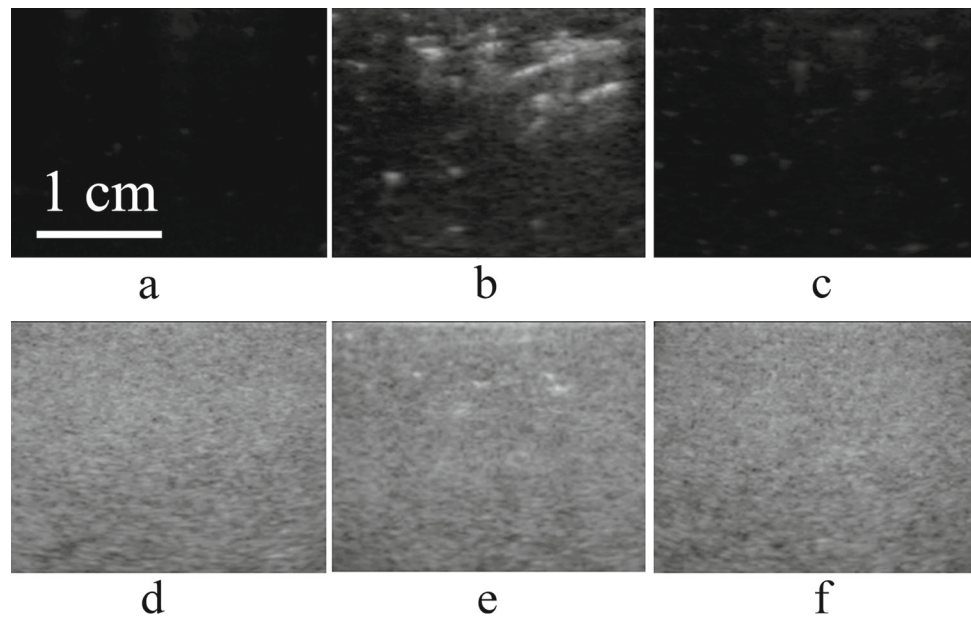
phantom is its capability to accurately replicate thyroid ultrasound anatomy, offering trainees an exceptionally realistic training experience. Different degrees of echogenicity were achieved in the phantom by incorporating varying concentrations of graphite powder and glitter. Thus, we reproduced the most relevant landmarks of the neck including carotid arteries, jugular veins, lymph nodes, and the thyroid gland with nodules (Figs. 3 and 4). Additionally, we introduced bone structures, produced as a single piece using high-resolution LCD resin 3D printer, thereby simplifying the manufacturing process, accelerating it, and improving the reproducibility of all phantom elements including relatively small and fragile structures such as the hyoid bone and cartilage. Upon analyzing the ultrasound images, it is evident that the modeled

structures are prominently displayed in all scans. However, images captured with more modern systems, such as shown in Fig. 4, exhibit clearer visualization of the modeled structures. This can be attributed to the advancements in equipment and incorporation of built-in image enhancing algorithms. When compared with other thyroid phantom designs [3–8], it could be noted that our model more accurately replicates ultrasound anatomy. This is because it is anthropomorphic and includes more elements of the human neck, all meticulously reproduced in the phantom, than any other model, including commercially available ones.

The material choice was based on acoustic properties (Fig. 5). Glandular and other tissues of the neck area including lesions were simulated using PVC plastisol, graphite powder, and glitter. The ultrasonic speed ranged from 1441 to 1473 m/sec, the coefficients of attenuation of ultrasound waves for the models of thyroid gland and the surrounding tissues were 0.95 and 0.58 dB/cm/MHz, respectively, which is in the range of values for the modeled human organs reported in the literature [12]. The phantom accurately reproduces tissue properties, providing adequate feedback to the trainees.

The fact that in our technology PVC is used as a base material makes the phantom long-lasting and storage friendly compared to designs incorporating ballistic gel, chicken breast, pickled fruits, and vegetables [4–7]. Moreover, the ultrasonic speed and attenuation in this material are within the range of human soft tissues, making it a perfect tool for practicing needle placement and estimating thyroid size.

Fig. 6 Ultrasound images of the tissue samples taken before (**a**, **d**), immediately after (**b**, **e**) and 15 min after the 100 insertions of a G21 needle accrued (**c**, **f**). The sample in images (a–c) is used to model vessels and cystic masses, while the sample in images (d–f) models tissues of normal echogenicity



The use of 3D printing with Industrial Blend resin and LCD technology for modeling bone structures has been justified due to several factors. First, the absence of chemical interaction between PVC materials, utilized for flexible structures, and the resin ensures the integrity and stability of the model. This allows for accurate representation of bone structures without any undesirable chemical reactions that may compromise its quality. Furthermore, the significant difference in acoustic impedance between PVC and the resin makes it an ideal choice for simulating bone structures. The selected resin for 3D printing had an ultrasound speed of 2.4 mm/ μ s and attenuation of 10 dB/cm/MHz, which is within the range for these parameters in human bones [14]. Finally yet importantly, manufacturing bone models using resins with LCD 3D printing technology allows avoiding the accumulation of air in crevices. If fused deposit modeling 3D printing were used instead of LCD technology, the accumulation of air between layers of filament would lead to air bubbles being trapped in PVC, distorting ultrasound images.

Table 2 clearly confirms that the dimensions of the models fall within the range of human organs as documented in the literature sources [10, 11]. It is evident that these dimensions vary according to factors such as sex, age, and weight. Therefore, it can be noted that our model accurately replicates a neck belonging to an overweight man over the age of 65.

The comparison between our phantom and actual ultrasound images of the human neck demonstrated similarity of the shape, size, brightness and position of the thyroid gland, carotid arteries, and bone structures. However, the jugular vein models in the phantom appeared larger than in the human neck. This discrepancy is attributed to the fact

that they were originally segmented from angiographic computed tomography data, where vessels are not compressed by an ultrasound probe. One advantage of our phantom design, setting it apart from previously reported designs [3–8], is the inclusion of a skin model. This not only enhances the accuracy of ultrasound images compared to human examination but also introduces a sensation of overcoming resistance to needle puncture, which ultimately brings the experience close to clinical practice.

For training with the neck phantom, the following steps are proposed:

(a) Preparation for work:

(1) Inspect the phantom thoroughly to ensure there is no mechanical damage.

(2) Gently place the phantom on a clean, flat, and horizontal work surface and ensure that all parts of the phantom are easily accessible by the transducer (Fig. 3a).

(3) If necessary, use a dry or damp cloth to wipe the phantom and remove any unwanted objects.

(4) Apply a water-based gel to either the phantom or transducer for clear visualization of the ultrasound image and smooth transducer glide.

(5) Adjust the ultrasound device according to the manufacturer's instructions.

(b) Ultrasound examination:

(1) Using the scheme in Fig. 1a, select the specific area or inclusion for visualization. For example, select an abnormal inclusion in the left lobe of the thyroid gland.

(2) Move the transducer over the phantom's surface to display the selected area or inclusion on the ultrasound device screen.

(3) Based on the ultrasound images of the thyroid gland, surrounding tissues, and any focal masses (Fig. 3b-f), prepare an ultrasound report. For instance, the location of the thyroid gland is typical, the shape is unchanged with clear contours. In the left lobe, there is a round nodule with decreased echogenicity measuring 6 mm. Enlarged lymph nodes can also be observed.

(4) Switch the device to elastography mode, evaluate the stiffness of the inclusions and make assumptions about the type of formation. For example, a cystic mass is detected in the left lobe.

(5) Prepare the needle for biopsy, determine the insertion path, and insert the needle according to the chosen trajectory.

(6) Collect the necessary material with the syringe, carefully remove it from the phantom and clean the surface of the phantom and ultrasound transducer.

One common limitation of medical phantoms is associated with the practice of fine-needle aspiration. If a sample is taken during aspiration, a permanent hole will be created in the phantom. Therefore, in order to extend the lifespan of the phantom, it is advisable to refrain from taking samples. Alternatively, if a needle is inserted without sampling, it may still leave a mark. To address this issue, an experiment was conducted involving the insertion of a G21 needle, commonly used in fine-needle aspiration, multiple times into the tissue of the phantom. Ultrasound images of the tissue were captured before and after the experiment. In Fig. 6, it can be observed that there were noticeable traces of the needle in images taken immediately after the insertion, and the traces were much more evident in the sample of anechoic tissue, compared to the sample of tissue with normal echogenicity. Due to the self-healing effect of the chosen material, over time the traces became less visible. Subsequently, in 15 min the number of needle marks decreased significantly, as evidenced by the ultrasound images in Fig. 6c and f. Therefore, it can be concluded that the phantom can withstand multiple needle insertions without losing its quality.

Although our design improves thyroid phantom development for ultrasound training, its major limitation is the lack of modeling muscle tissues. This is a common problem for all thyroid phantom designs presented in the literature [3–8]. Thus, in the future we plan to add a muscle tissue model between the thyroid gland and the skin to make ultrasound experience with the phantom more realistic. Those who would like to reproduce the results of our research are advised to use our data [15].

Conclusions

The proposed manufacturing technology provides a reliable and cost-effective approach to fabricating an anthropomorphic neck phantom for ultrasound diagnosis of the thyroid

gland. In order for the phantom to accurately represent human anatomy, the angiographic computed tomography data were used to put in place vessels, bone structures, and other anatomical landmarks. The realistic simulation offered by the phantom enhances the quality and accuracy of ultrasound examinations, facilitating better training of medical professionals and improving patient care. Future research can focus on refining the fabrication process and exploring additional features to enhance the phantom's capabilities.

Acknowledgements This paper was prepared by a group of authors as a part of the research and development effort titled “Scientific rationale for development and use of tissue-equivalent materials to design test objects for radiology” (USIS No.:№ 123092000013-3) in accordance with the Order No. 1196 dated December 21, 2022 “On approval of state assignments funded by means of allocations from the budget of the city of Moscow to the state budgetary (autonomous) institutions subordinate to the Moscow Healthcare Department, for 2023 and the planned period of 2024 and 2025” issued by the Moscow Healthcare Department. The authors would like to express their gratitude to Daria Leichenko for her contribution at the preliminary stage of the research.

Declarations

Competing interest The authors declare that they have no known competing financial interests or personal relationships that could have appeared to influence the work reported in this paper.

References


1. Siegel RL, Miller KD, Wagle NS (2023) Jemal A (2023) Cancer statistics. *CA Cancer J Clin* 73(1):17–48. <https://doi.org/10.3322/caac.21763>
2. Alexander LF, McComb BL, Bowman AW, Bonnett SL, Ghazanfari SM, Caserta MP (2023) Ultrasound simulation training for radiology residents—curriculum design and implementation. *J Ultrasound Med* 42(4):777–790
3. Boers T, Brink W, Bianchi L, Saccomandi P, van Hespen J, Wennemars G, Braak S, Versluis M, Manohar S (2023) An anthropomorphic thyroid phantom for ultrasound-guided radiofrequency ablation of nodules. *Med Phys*. <https://doi.org/10.1002/mp.16906>
4. Hakimi AA, Armstrong WB (2021) Improving on the do-it-yourself ultrasound-guided fine-needle aspiration simulation phantom. *J Ultrasound Med* 40(4):815–819
5. Cheng A, Lee JWK, Ngiam KY (2023) Use of 3D ultrasound to characterise temporal changes in thyroid nodules: an in vitro study. *J Ultrasound* 26(3):643–651
6. Phillips H, Franklin C, Brearley J, Holmes M, Genain MA (2023) Natural ballistic gelatine ultrasound phantoms are suitable to be used for student education and can be produced cheaply and effectively. *Vet Radiol Ultrasound* 64(4):733–739. <https://doi.org/10.1111/vru.13235>
7. Schwartz CM, Ivancic RJ, McDermott SM, Bahner DP (2020) Designing a low-cost thyroid ultrasound phantom for medical student education. *Ultrasound Med Biol* 46(6):1545–1550
8. Baba M, Matsumoto K, Shindo H, Matsumoto M, Otsubo R, Tanaka A, Oyama S, Zhu R, Yamamoto I, Nagayasu T (2023) Development and evaluation of an original phantom model of ultrasonography-guided thyroid gland biopsy for the training of surgical residents and students. *Surg Today* 53(4):443–450

9. Leonov D, Venidiktova D, Costa-Junior JFS, Nasibullina A, Tarasova O, Pashinceva K, Vatsheva N, Bulgakova J, Kulberg N, Borsukov A, Saikia MJ (2023) Development of an anatomical breast phantom from polyvinyl chloride plastisol with lesions of various shape, elasticity and echogenicity for teaching ultrasound examination. *Int J Comput Assist Radiol Surg*. <https://doi.org/10.1007/s11548-023-02911-4>
10. Fritze F, Groß S, Ittermann T, Völzke H, Felix SB, Schminke U, Dorr M, Bahls M (2020) Carotid lumen diameter is associated with all-cause mortality in the general population. *J Am Heart Assoc* 9(16):e015630
11. Lee MK, Na DG, Joo L, Lee JY, Ha EJ, Kim JH, Jung SL, Baek JH (2023) Standardized imaging and reporting for thyroid ultrasound: korean society of thyroid radiology consensus statement and recommendation. *Korean J Radiol* 24(1):22–30. <https://doi.org/10.3348/kjr.2022.0894>
12. Duck FA (1990) Physical properties of tissue: a comprehensive reference book. Academic Press
13. Matheo LL, Geremia J, Calas MJ, Costa JF, Silva FF, Krüger MA, Pereira WC (2018) PVC-based anthropomorphic breast phantoms containing structures similar to lactiferous ducts for ultrasound imaging: a comparison with human breasts. *Ultrasonics* 90:144–152. <https://doi.org/10.1016/j.ultras.2018.06.013>
14. Leonov D, Kodenko M, Leichenko D, Nasibullina A, Kulberg N (2022) Design and validation of a phantom for transcranial ultrasonography. *Int J Comput Assist Radiol Surg* 17(9):1579–1588. <https://doi.org/10.1007/s11548-022-02614-2>
15. STL files for 3D printing neck phantom molds. https://www.researchgate.net/publication/378875793_STL_files_for_3D_printing_neck_phantom_molds

Publisher's Note Springer Nature remains neutral with regard to jurisdictional claims in published maps and institutional affiliations.

Springer Nature or its licensor (e.g. a society or other partner) holds exclusive rights to this article under a publishing agreement with the author(s) or other rightsholder(s); author self-archiving of the accepted manuscript version of this article is solely governed by the terms of such publishing agreement and applicable law.

Authors and Affiliations

Denis Leonov^{1,2}  · Anastasia Nasibullina¹  · Veronika Grebennikova^{1,2}  · Olga Vlasova¹  · Yulia Bulgakova^{1,2}  · Ekaterina Belyakova^{1,3}  · Darya Shestakova⁴  · José Francisco Silva Costa-Júnior⁵  · Olga Omelianskaya¹  · Yuriy Vasilev¹ 

✉ Denis Leonov
strat89@mail.ru

Anastasia Nasibullina
NasibullinaAA@zdrav.mos.ru

Veronika Grebennikova
GrebennikovaVV@zdrav.mos.ru

Olga Vlasova
VlasovaOV10@zdrav.mos.ru

Yulia Bulgakova
BulgakovaYV@zdrav.mos.ru

Ekaterina Belyakova
BelyakovaED@zdrav.mos.ru

Darya Shestakova
daria@venidiktova.ru

José Francisco Silva Costa-Júnior
francisco@sbeb.org.br

Olga Omelianskaya
OmelyanskayaOV@zdrav.mos.ru

Yuriy Vasilev
VasilevYA1@zdrav.mos.ru

- 1 Moscow Center for Diagnostics and Telemedicine, Moscow, Russia
- 2 Moscow Power Engineering Institute, Moscow, Russia
- 3 Sechenov University, Moscow, Russia
- 4 Smolensk State Medical University, Moscow, Russia
- 5 Brazilian Air Force Academy, Pirassununga, São Paulo, Brazil